Biosensors and Bioelectronics 28 (2011) 428–433

Contents lists available at ScienceDirect

Biosensors and Bioelectronics

journal homepage: www.elsevier.com/locate/bios

Detection of ricin using a carbon nanofiber based biosensor

Adaikkappan Periyakaruppan, Prabhu U. Arumugam[1], M. Meyyappan, Jessica E. Koehne*

NASA Ames Research Center, Moffett Field, CA 94035, USA

ARTICLE INFO

Article history:
Received 9 April 2011
Received in revised form 11 July 2011
Accepted 25 July 2011
Available online 31 July 2011

Keywords:
Ricin
Carbon nanofiber
Antibody
Aptamer
Electrochemical impedance spectroscopy

ABSTRACT

We report ricin detection using antibody and aptamer probes immobilized on a nanoelectrode array (NEA) consisting of vertically aligned carbon nanofibers (VACNFs). These biosensor chips are fabricated on a wafer scale using steps common in integrated circuit manufacturing. Electrochemical impedance spectroscopy is used to characterize the detection event and the results indicate that the electron transfer resistance changes significantly after the ricin protein binds to the probe. Further confirmation is obtained from evaluation of the electrode surface by atomic force microscopy which clearly shows a change in height from the bare electrode to the surface bound by the probe-protein.

Published by Elsevier B.V.

1. Introduction

Ricin is a toxic glycoprotein readily isolated from the castor bean seeds *Ricinus communis*. It consists of two chains (A and B) roughly of equal size that are connected by a disulfide bond, with a total molecular weight of ~62 kDa. The B chain is essential for binding to the cell surface and it transports the A chain into the cytosol. The A chain is toxic to cells which stops protein production, thus leading to cell death. Ricin is classified as a bio-warfare agent and its ready availability is a major concern in terrorism. Detection of ricin and other bio-threats has been an active subject of interest in the last decade, and recent reviews (Gooding, 2006; Ler et al., 2006; Skottrup et al., 2008; Vikesland and Wigginton, 2010) provide an overview of analytical techniques and biosensors reported in the literature for this purpose, detection results and limits, comparison of available methods and a comprehensive list of references. A waveguide based biosensor array was reported for the detection of bacteria and protein toxins wherein the resultant patterns due to antibody–antigen interactions from the array are captured by a CCD camera (Rowe-Taitt et al., 2000a,b; Wadkins et al., 1998). This array was shown to be capable of detecting ricin down to 25 ng/mL. A microarray of individually addressable electrodes based on conventional complementary metal oxide semiconductor (CMOS) circuitry was used by Dill et al. (2004) for ricin detection at ~5 ng/mL. An "electronic tongue" setup containing a fluid delivery system, flow cell, fluorescence microscope, and a digital camera was used as aptamer biosensor for detection and quantification of proteins (Kirby et al., 2004) and a limit of detection of 320 ng/mL was reported using this sensor. An affinity based electrophoresis also using aptamers was demonstrated to be useful for the sensitive identification of ricin at ~14 ng/mL (Haes et al., 2006). Interesting concepts such as biological signal amplification in a well-in-a-well type of device have been reported for detection as well as measuring the toxicity level of ricin after physical or chemical treatment (Mei et al., 2006). Miniaturization of the detection system for field-deployable needs was achieved by a hand-held surface Plasmon resonance biosensor which was able to detect ricin at 200 ng/mL in 10 min (Feltis et al., 2008).

In spite of the impressive demonstrations in the literature, small, inexpensive, multiplexed biosensors capable of sensitive detection of ricin and other biothreats is not currently available. In this regard, chip based sensor systems, for example a bioFET (field effect transistor), have not been reported for ricin detection as these are amenable for low cost manufacturing. Likewise, advantages of emerging nanomaterials such as carbon nanotubes (CNTs), graphene, and various inorganic nanowires in terms of their interesting electrical, optical, and other properties have not been exploited either. Both single and multi-walled CNTs have been used for the construction of amperometric and potentiometric biosensors for various applications (Lin et al., 2004; Suresh et al., 2010; Wang, 2005). We have reported biosensors using vertically aligned carbon nanofibers (VACNFs) that are 30–50 nm in diameter (Koehne et al., 2004; Li et al., 2005; Arumugam et al., 2010). These individual, freestanding nanostructures are amenable to

* Corresponding author. Tel.: +1 650 604 6818.
E-mail address: Jessica.E.Koehne@nasa.gov (J.E. Koehne).
[1] Present address: Advanced Diamond Technologies, Inc., #429B Weber Road, #286, Romeoville, IL 60446, USA.

0956-5663/$ – see front matter. Published by Elsevier B.V.
doi:10.1016/j.bios.2011.07.061

construct nanoelectrode arrays (NEAs) with a predefined distance between individual electrodes, thus offering processing advantages over randomly grown nanotubes, nanowires or graphene. Here we combine the advantages of VACNFs with wafer scale fabrication of nanoelectrode arrays to develop reusable nano-biosensors for biothreat detection.

2. Experimental

2.1. Sensor fabrication

Individual, freestanding, vertically aligned carbon nanofibers (VACNFs) grown by plasma-enhanced chemical vapor deposition (PECVD) on a silicon wafer serve as nanoelectrodes. Fig. 1 shows a representative scanning electron microscopy (SEM) image of a VACNF array. Though individual CNF nanoelectrodes can be precisely positioned using lithographic patterning, the present demonstration utilizes a randomly grown CNF array wherein the average distance between adjacent electrodes is about 1 μm. Growth of the VACNF array and fabrication details have been reported previously (Koehne et al., 2004; Li et al., 2005) and only a brief account is given below.

A 200 nm chromium layer was sputtered onto a silicon wafer with 500 nm thick thermal oxides followed by a thin layer of nickel (30 nm) sputtered as catalyst. A dc-biased PECVD system was used to grow VACNFs with acetylene as feedstock (125 sccm) and ammonia as diluent (444 sccm) at 6.3 mbar, 700 °C, and 180 W power. The VACNFs are typically 100 nm in diameter at the bottom and 80 nm at the tip and are ~3 μm tall for a growth time of 15 min. Individual VACNFs were electrically isolated from each other by depositing SiO_2 as a dielectric using chemical vapor deposition (CVD) with tetraethoxysilane as precursor. The oxide completely encapsulates each fiber. A subsequent chemical mechanical polishing (CMP) step provides a smooth SiO_2 top surface with only tips of the VACNFs protruding above the surface. As-grown VACNFs and the nanoelectrode array after CMP were characterized by field emission scanning electron microscopy (SEM) (S4800, Hitachi, Pleasanton, CA) as shown in Fig. 1.

2.2. Electrochemical characterization

The VACNFs chip prepared as above were characterized electrochemically prior to their use in ricin detection. They were pretreated by soaking in 1.0 M HNO_3 for 15–30 min and washed with sterile water prior to electrochemical characterization for several reasons: removal of damage, if any, to the VACNF tips during various fabrication processing steps, improving electrode kinetics, and introducing –COOH groups for subsequent covalent binding of the antibody or aptamer probe for biosensor development. Electrochemical properties of bare unmodified VACNFs chips were evaluated through cyclic voltammetry (CV) and impedance spectroscopy (EIS) (Siddiqui et al., 2010). The cyclic voltammograms (CV) were recorded between −0.4 and 0.8 V vs. SCE (saturated calomel electrode) with a scan rate of 20 mV/s in a solution of 5 mM $K_4Fe(CN)_6$/5 mM $K_3Fe(CN)_6$ in 0.1 M phosphate buffer (pH 7.4) (1:1 mixture). EIS measurements were carried out in a mixture of 5 mM $K_4Fe(CN)_6$/5 mM $K_3Fe(CN)_6$ in 0.1 M KCl using a CHI potentiostat/galvanostat equipped with a Frequency Response Analyzer module (CHI 660D, Austin, TX). The spectra were taken at 0.1 Hz–100 kHz at open circuit potential vs. SCE (saturated calomel electrode) reference electrode.

2.3. Detection using ricin-A antibody

A 5 μL of (1:500 dilution) ricin-A antibody (rcE-19, Santa Cruz BioTech.) in a 50 μL phosphate buffered saline (PBS) containing 1 mM magnesium chloride mixed with a coupling reagent of 0.5 mg N-(3-dimethylaminopropyl)-N′-ethylcarbodiimide hydrochloride (EDC) and 0.25 mg N-hydroxysulfosuccinimide sodium salt (NHS). The reaction mixture was placed on a VACNF chip and incubated at room temperature for 2 h. The primary amine groups in the Ricin A antibody form amide bonds with the carboxyl-groups at the VACNF tips. Nonspecific binding was eliminated by stringent wash in three steps using (1) 2× SSC (saline sodium citrate)/0.1% SDS (sodium dodecyl sulfate), (2) 1× SSC, and (3) 0.1× SSC by shaking the VACNF chip in each solution for 15 min at room temperature respectively. The ricin-A antibody binding to the VACNFs chip was evaluated through CV and EIS.

The target capture binding was carried out by incubating the ricin-A antibody-functionalized electrodes in 5 μL of 0.5 μg/mL ricin protein (L-9514, Sigma–Aldrich) or 5 μL of 5 μg/mL collagen as control protein (C-9791, Sigma–Aldrich) with 50 μL of PBS buffer incubated at room temperature for 1 h. The electrodes were then washed in three stringent steps with buffers (1) 2× SSC/0.1% SDS, (2) 1× SSC, and (3) 0.1× SSC by shaking the chip in each solution for 15 min at room temperature and the nonspecific binding of proteins was eliminated. The target ricin protein binding was also evaluated by CV and EIS.

2.4. Detection using ricin aptamer

A 5 μL of 0.12 μg/mL anti-ricin (Aricin) RNA Aptamer (31RA) with a sequence 5′-NH_2-C6-5′-/5AmMC6/GGC GAA UUC AGG GGA CGU AGC AAU GAC UGC C-3′ (Fan et al., 2008) (Sigma-Genosys) in a 50 μL PBS buffer containing 1 mM magnesium chloride was mixed with a coupling reagent of 0.5 mg EDC + 0.25 mg of NHS. The reaction mixture was placed on a VACNF chip and incubated for 2 h at 40 °C. The presence of Mg^{2+} has been shown to be necessary for the interaction between the aptamers and proteins. Nonspecific binding was eliminated by stringent wash in three steps using (1) 2× SSC/0.1% SDS, (2) 1× SSC, and (3) 0.1× SSC by shaking the chip in each solution for 15 min at room temperature. The immobilized Aricin RNA aptamer binding to the VACNFs chips was evaluated through CV and EIS.

The target binding was carried out by incubating the Aricin RNA aptamer-functionalized electrodes in 5 μL of 0.5 μg/mL ricin protein with 50 μL of PBS buffer incubated at room temperature for 1 h. The electrodes were then washed to eliminate nonspecific binding with (1) 2× SSC/0.1% SDS, (2) 1× SSC, and (3) 0.1× SSC by shaking the chip in each solution for 15 min at room temperature. The target ricin protein binding to the probes in VACNFs chips was evaluated through CV and EIS. The entire process was repeated with a nonspecific control using 5 μL of 0.78 μg/mL DNA aptamer with a sequence 5′-CCC CGT GCG GTG ATC CTC CCT GCC TAT TTG CAC GGG G-NH_2-3′.

Reactivation of aptamer was attempted by heat denaturation of Aricin at 70 °C for 3 min and the entire target capture procedure was repeated to assess the efficacy. Aptamer regeneration was performed by washing the corresponding VACNF chip with an elution buffer (100 mM sodium citrate, 10 mM EDTA, 7 M urea, pH 5.0) for removal of the ricin protein and then, the reusability of Aricin aptamer was checked several times using EIS.

2.5. Atomic force microscopy characterization

The topography of the sensors was characterized using a Nanoscope Multimode atomic force microscope (AFM) (Digital Instruments, Santa Barbara, CA) in order to further identify probe and target binding. AFM images were acquired in contact mode using an ORC8 silicon nitride cantilever with a 0.1 N/m spring constant (Veeco, Santa Barbara, CA). Scan rates were typically 1.0 Hz and data was collected with 512 × 512 pixels/frame. Height and

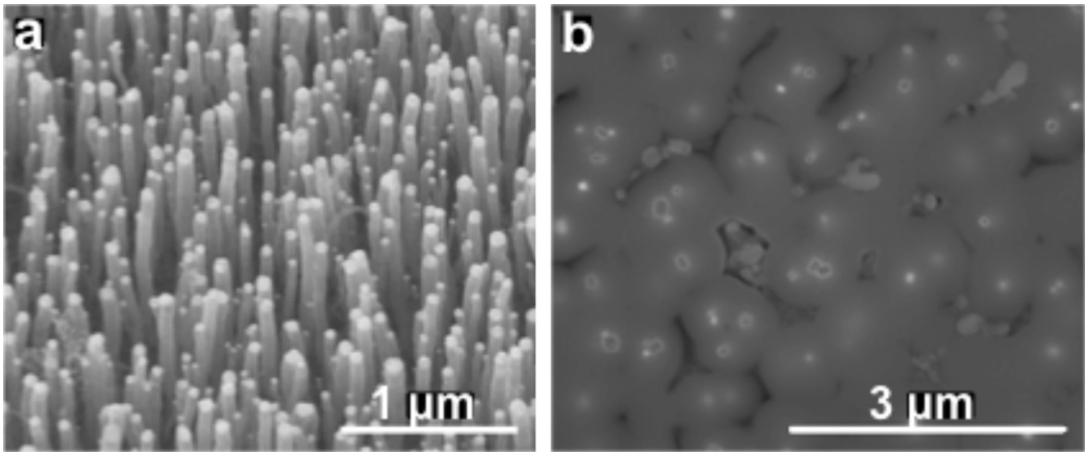

Fig. 1. Scanning electron microscopy images of carbon nanofiber arrays. (a) An array of as-grown vertically aligned carbon nanofibers (VACNF). (b) VACNF nanoelectrode array (NEA) after SiO_2 deposition and chemical mechanical polishing.

deflection data were acquired simultaneously and feature height was measured using the section analysis tool in the Multimode software. Thirty feature height measurements were taken for each experiment and mean and standard deviations were calculated. All probe and target binding experiments were characterized by AFM, a minimum of two times, in order to further verify observations.

3. Results and discussion

The size and separation of individual VACNF electrodes in the NEA are key parameters to ensure nanoelectrode performance (Siddiqui et al., 2010). SEM images of as-grown VACNFs and the electrode array with VACNFs embedded in silicon dioxide to make the NEA and are shown in Fig. 1. The as-grown VACNFs are well aligned, approximately 3 μm tall and have diameters ranging from 50 to 100 nm. Fig. 1b also clearly shows that each nanofiber is completely encapsulated by SiO_2. After SiO_2 encapsulation and CMP, the mean separation distance between individual electrodes is approximately 700 nm, which is ideal to maintain non-overlapping hemispherical diffusion layers around each VACNF. Steady state cyclic voltammograms serve as further confirmation of ideal VACNF NEA separation. Each VACNF NEA chip in this study shows steady state behavior in 5 mM $K_4Fe(CN)_6$/5 mM $K_3Fe(CN)_6$ in 0.1 M phosphate buffer (pH 7.4) (1:1 mixture).

Cyclic voltammetry characterization of VACNF NEAs sequentially modified with the probe and the target were done in 2 mM $K_3Fe(CN)_6$ in 0.1 M phosphate buffer (pH 7.4) and the results are shown in Fig. 2. The $Fe(CN)_6^{3-}/^{4-}$ shows a reversible one-electron redox peak in the bare VACNF NEA. A substantial decrease in overall current is observed upon immobilization of the probe (antibody or aptamer) on the VACNF electrode, due to the physical blockage of the electrode surface by the probe. Upon target binding, the current in the CV scans increases slightly, again suggesting a change in the electron transfer at the electrode's surface. These changes in CV responses of bare/probe/target provide evidence that efficient probe immobilization and target hybridization occurred on the VACNF electrode surface.

Probe immobilization to the VACNF chip and probe-target bindings were characterized by EIS and changes in the electron transfer resistance of the electrode R_{ct} were monitored. Fig. 3 shows Nyquist plots for the VACNF-based biosensor using probes ricin-A antibody and Aricin RNA aptamer. The R_{ct} increases with the immobilization of the ricin-A antibody probe to the VACNF electrode surface, resulting from the presence of a bio-layer. Further increase in resistance is seen upon binding of the target ricin protein, shown in Fig. 3a. In contrast, when a control collagen protein was incubated on the VACNF chip immobilized with the ricin-A antibody, the R_{ct} value does not increase, indicating that the collagen protein is not successfully captured by ricin-A antibody probe (Fig. 3c). The observation of decreasing R_{ct} value suggests that some of the immobilized ricin-A antibody probes were removed, possibly resulting from antibody degradation or noncovalently bound layers of ricin-A antibody on the VACNF surface. Further washing of the functionalized chip produced a gradual decrease in R_{ct} values, indicating that antibody probes may have limited stability and shelf-life (Jayasena, 1999).

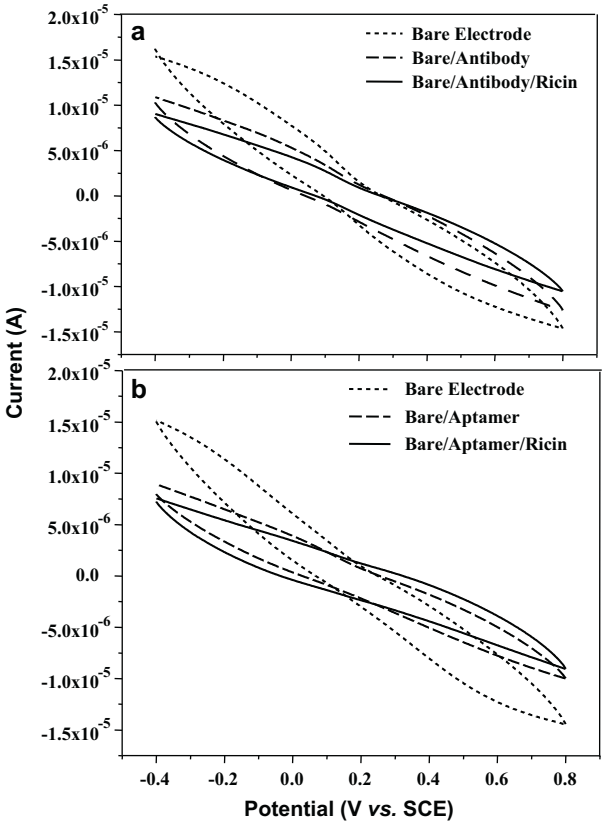

Fig. 2. Cyclic voltammetry analysis of VACNF electrode in the presence of 2 mM $K_3[Fe(CN)_6]$ and 0.1 M KCl. (a) Sequential modification of VACNF NEA with ricin-A antibody and then target ricin. (b) Sequential modification of VACNF NEA with Aricin RNA aptamer and then target ricin.

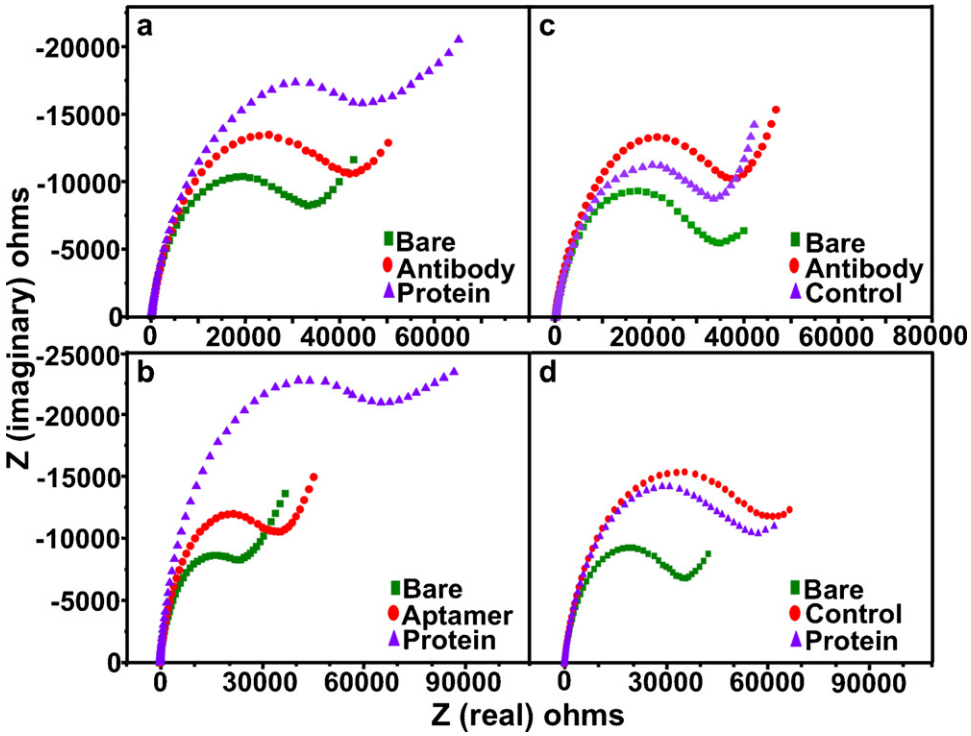

Fig. 3. Impedance spectra for ricin detection using antibody and aptamer probes. Bare VACNF NEA is shown in green, bound probe is shown in red and the purple curve represents the VACNF after exposure to the target molecules. (a) EIS spectra of antibody probe and ricin target, (b) EIS spectra of antibody probe and control target, (c) EIS spectra of ricin aptamer probe and ricin target, (d) EIS spectra of control aptamer probe and ricin target. (For interpretation of the references to color in this figure legend, the reader is referred to the web version of the article.)

Fig. 3b represents the corresponding impedance spectra for aptamer-based ricin detection. The Aricin aptamers are much smaller (10 kDa) than the ricin-A antibody (32 kDa) and more specific towards their targets, which allow a much more pronounced signal upon ricin binding. An increase in R_{ct} value is seen after the immobilization of the Aricin aptamer on the bare NEA. The change in R_{ct} value is substantial after ricin protein is bound to the Aricin aptamer, indicating successful detection of ricin protein binding. Here again, when a control aptamer was used, a small decrease in R_{ct} value was observed upon exposure to Aricin, indicating a lack of target binding (Fig. 3d).

Aptamers have shown the ability to maintain bioactivity after denaturation (Kirby et al., 2004) and here, we demonstrate this in ricin detection. Fig. 4 contains Nyquist plots of a sensor chip after reactivation of denatured Aricin aptamer. The R_{ct} value noticeably decreases after washing with elution buffer which removes the ricin target protein and returns to a value comparable to that of the original Aricin aptamer functionalized chip. This indicates that the ricin protein can be washed away but the Aricin aptamer probe remains bound to the VACNFs. Upon reintroduction to ricin, R_{ct} increases to a value similar to the original ricin-bound EIS curve. This process was repeated several times with highly reproducible results as shown for the first cycle in Fig. 4. This observation proves that the aptamer retains its bioactivity and is able to be regenerated, thus indicating the reusability of the aptamer based biosensor.

Probe and target binding were further confirmed using atomic force microscopy by monitoring the changes in feature height after probe immobilization and target exposure. Fig. 5 represents 3-dimensional height topographs for the sensor chips. Features protruding from the silicon dioxide are observed prior to probe immobilization (Fig. 5a and d), which is consistent with previous results (Li et al., 2005). These features grow substantially upon immobilization of probe molecules and then again after target binding as seen in Fig. 5. The typical dimensions of ricin-A chain proteins are approximately 8.76 nm × 6.78 nm × 6.16 nm (Robertus et al., 1996). Molecular graphics images were produced using the UCSF Chimera package from the Resource for Biocomputing, Visualization, and Informatics at the University of California, San Francisco (Gestwicki et al., 2002) (supported by NIH P41 RR-01081). Height analysis of the AFM topographs indicates that the introduction of ricin-A chain protein resulted in multilayer adsorption on the probe functionalized NEAs. The AFM characterization provides a further

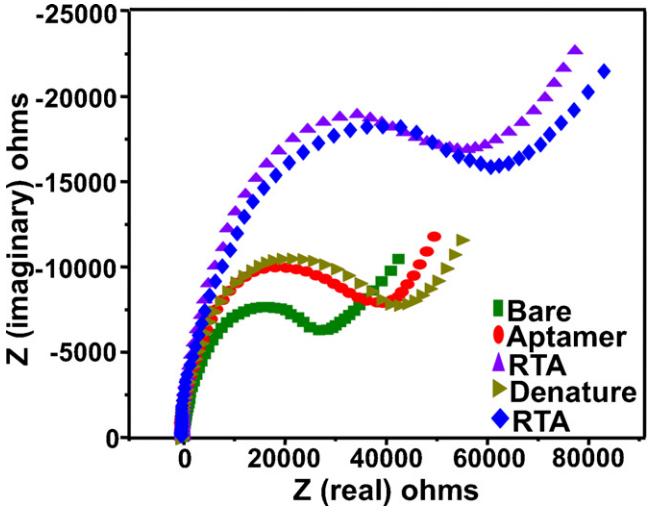

Fig. 4. Impedance spectra of reused aptamer-based ricin detection chip. Green curve represents the bare, unmodified VACNF NEA. The red curve represents the binding with the aptamer probe. The purple curve represents the ricin target aptamer (RTA). The brown curve represents the NEA after aptamer denaturization. The blue curve represents the rebinding of the ricin target aptamer (RTA). (For interpretation of the references to color in this figure legend, the reader is referred to the web version of the article.)

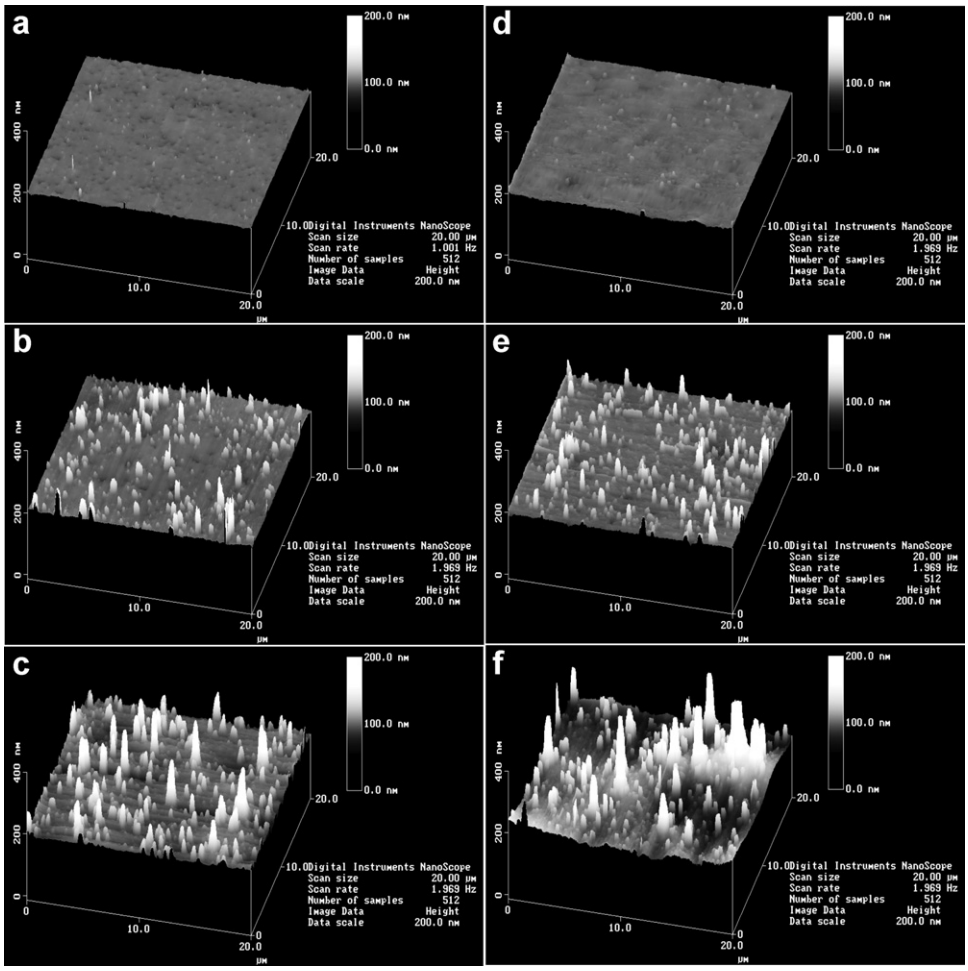

Fig. 5. 3-Dimensional AFM surface topography of the VACNF NEA. (a) Bare electrode, (b) after immobilization with antibody probe, (c) after target ricin protein binding to the antibody probe, (d) bare electrode, (e) after immobilization with aptamer probe, and (f) after ricin protein binding to the antibody.

confirmation of the EIS observation by showing a change in surface topography of the electrode after probe immobilization and protein binding from that of the bare electrode.

4. Conclusion

We have developed a carbon nanofiber based nanoelectrode array suitable for the detection of biothreat agents. The electrochemical impedance spectra clearly indicate a substantial change in electron transfer resistance R_{ct} values after the binding of ricin protein to antibody and aptamer probes; in the case of the latter, the signal is much stronger. While the ricin-A antibody probe is insufficiently bound to the VACNFs, the Aricin aptamer probe is stable and can be regenerated multiple times to create a reusable biosensor. In our current effort, we are already able to fabricate the biosensor chips on 4 inch wafers and the process is scalable to larger wafer sizes. Further work is needed to establish the low detection limits in pM range, which depends on controlling the spacing between individual VACNFs; i.e., a patterned nanoelectrode array with spacing to match the scenario of individual isolated electrodes (to avoid overlapping of radial diffusion layers) would significantly improve the sensitivity, in contrast to the forest-like electrodes with random spacing in the present work. Other useful changes may include better dielectric for isolation, for example, parylene (Arumugam et al., 2010) and reducing the interfacial resistance at the CNF-substrate interface. A deployable small scale system would require integration of micro-fluidics to the sensor and a signal processing chip for electrochemical analysis.

Acknowledgements

The authors acknowledge Prof. Nader Pourmand and Dr. Paolo Actis of University of California Santa Cruz for providing the aptamers used in this work and Dr. Olufisayo Jejelowo of Texas Southern University and Dr. Govindarajan Ramesh of Norfolk State University for their support. Adaikkappan Periyakaruppan is a Postdoctoral Fellow from Texas Southern University, Houston, supported by a NASA URC contract to TSU, NNX08BA47A. This work was supported in part by the Department of Homeland Security through contract IAA: HSHQDC-08-X-00870.

References

Arumugam, P.U., Yu, E., Riviere, R., Meyyappan, M., 2010. Chem. Phys. Lett. 499, 241–245.
Dill, K., Montgomery, D.D., Ghindilis, A.L., Schwarzkopf, K.R., Ragsdale, S.R., Oleinikov, A.V., 2004. Biosens. Bioelectron. 20, 736–742.
Fan, S., Wu, F., Martiniuk, F., Hale, M.L., Ellington, A.D., Tchou-Wong, K.M., 2008. World J. Gastroenterol. 7 (41), 6360–6365.
Feltis, B.N., Sexton, B.A., Glenn, F.L., Best, M.J., Wilkins, M., Davis, T.J., 2008. Biosens. Bioelectron. 23, 1131–1136.
Gestwicki, J.E., Cairo, C.W., Mann, D.A., Owen, R.M., Kiessling, L.L., 2002. Anal. Biochem. 305, 149–155.

Gooding, J.J., 2006. Anal. Chim. Acta 559, 137–151.
Haes, A.J., Giordano, B.C., Collins, G.E., 2006. Anal. Chem. 78, 3758–3764.
Jayasena, S.D., 1999. Clin. Chem. 9 (45), 1628–1650.
Kirby, R., Cho, E.J., Gehrke, B., Bayer, T., Park, Y.S., Neikirk, D.P., McDevitt, J.T., Ellington, A.D., 2004. Anal. Chem. 76, 4066–4075.
Koehne, J., Li, J., Cassel, A.M., Chen, H., Ye, Q., Ng, H.T., Han, J., Meyyappan, M., 2004. J. Mater. Chem. 14, 676–684.
Ler, S.G., Lee, F.K., Gopalakrishnakone, P., 2006. J. Chromatogr. A 1133, 1–12.
Li, J., Koehne, J., Cassel, A.M., Chen, H., Ye, Q., Ng, H.T., Fan, W., Meyyappan, M., 2005. Electroanalysis 17, 15–27.
Lin, Y., Lu, F., Tu, Y., Ren, Z., 2004. Nano Lett. 4, 191–195.
Mei, Q., Fredrickson, C.K., Lian, W., Jin, S., Fan, Z.H., 2006. Anal. Chem. 78, 7659–7664.
Robertus, J.D., Yan, X., Ernst, S., Monzingo, A., Worley, S., Day, P., Hollis, T., Svinth, M., 1996. Toxicon 34 (11-12), 1325–1334.
Rowe-Taitt, C.A., Golden, J.P., Feldstein, M.J., Cras, J.J., Hoffman, K.E., Ligler, F.S., 2000a. Biosens. Bioelectron. 14, 785–794.
Rowe-Taitt, C.A., Hazzard, J.W., Hoffman, K.E., Cras, J.J., Golden, J.P., Ligler, F.S., 2000b. Biosens. Bioelecton. 15, 579–589.
Siddiqui, S., Arumugam, P.U., Chen, H., Li, J., Meyyappan, M., 2010. ACS Nano 4, 955–961.
Skottrup, P.D., Nicolaisen, M., Justesen, A.F., 2008. Biosens. Bioelecton. 24, 339–348.
Suresh, S., Gupta, A.K., Rao, V.K., Kumar, O., Vijayaraghavan, R., 2010. Talanta 81, 703–708.
Vikesland, P.J., Wigginton, K.R., 2010. Environ. Sci. Technol. 44, 3656–3669.
Wadkins, R.M., Golden, J.P., Pritsiolas, L.M., Ligler, F.S., 1998. Biosens. Bioelectron. 13, 407–415.
Wang, J., 2005. Electroanalysis 17, 7–14.